2020 SCEC Proposal – Final Report

EARTHQUAKE GATES: INVESTIGATING THE ROLE OF SEISMIC WAVES IN MULTI-FAULT RUPTURING

Principal Investigators:
Hector Gonzalez-Huizar (PI)

University of Texas at El Paso
Department of Geological Sciences 500
W. University Ave.
El Paso, TX 79968-0555
Phone: (915)-747-5305
E-mail: hectorg@miners.utep.edu

Co-Principal Investigators:
Roby Douilly (co-PI)

University of California, Riverside Department
of Earth and Planetary Sciences 900
University Ave.
Riverside, CA, 92521
Phone: (951)-827-2976
E-mail: roby.douilly@ucr.edu

Amount of Requested Funding: $38,773

Proposal Category: Category 3.2.2.A Collaborative Proposal

Science Priority Objectives and Thematic Areas: Earthquake gates, SCEC5

Start Date: February 1, 2020

A. Introduction:

Under this project, we investigated potential scenarios in which a rupture originated along the San Jacinto Fault propagates onto the San Andreas Fault. Specifically, our focus was on investigating the role of seismic waves in the propagation of the rupture, through dynamic triggering mechanisms. Dynamic triggering on a fault occurs when the passing of seismic waves alters the mechanical state or properties of the fault, weakening it and promoting its failure [*Hill* 2012a,b]. Recent studies have shown that in some cases of multi-fault ruptures the seismic waves generated by the failure in one of the faults plays an important role in triggering the failure of the subsequent faults. That is, in cases of multi-fault ruptures where the distance between the ruptured faults is too large (several fault's lengths) so that the slip of the first fault causes static stress changes on the second fault insufficient to promote its failure; triggering, or at least the weakening, of the second fault by the seismic waves from the first one, is a plausible mechanism. For example, Zhang et al [2012] suggest that the 2012 Mw 8.6 Sumatra earthquake, the greatest strike-slip earthquake ever recorded, was the result of the successive rupture of three different faults. They argue that the initiation of the rupture of the second fault could be statically and dynamically triggered by the first fault, however, the third fault was primary dynamically triggered by the *S* or Love waves radiated from the second fault. Similarly, Nisse et al [2016] show that a Mw 7.1 earthquake occurred in Pakistan was a doublet initiated on a shallow blind reverse fault, followed 19 s later by a second rupture on a separated reverse fault 50 km away. From the analysis of geodetic and seismic data they infer that static Coulomb stresses at the initiation location of the second earthquake were reduced as result of the first; suggesting that a dynamic triggering mechanism initiating the rupture in the second fault is a possible mechanism. Other potential cases of multi-fault ruptures where seismic waves played an important role include the 1032, Mw 7.6 Chang Ma, China earthquake and the 1896, Mw 7.5 Riku, Japan earthquake, which contain faults gaps of 10 km and 15 km, respectively [Rubin, 1996]. Potential cases of multi-segment and multi-fault rupture in the San Andreas Fault system have been reported [see e.g., Dolan et al 1995, Lozos 2016]; as well as many cases of earthquakes, non-volcanic tremor, and slow-slip events, promoted by the transient stresses. Under this SCEC project, we evaluated the role of seismic wave-related stress in promoting multi-fault ruptures, specifically, in a potential propagation of a rupture on the San Jacinto Fault (SJF) onto the San Andreas Fault (SAF). We used the spontaneous finite element code FaultMod [Barall, 2009] to model several scenarios of earthquakes with different geometries of the SAF and SJF and investigated the potential weakening that seismic waves from a rupture in the SJF could cause along the SAF, and its role in facilitating the propagations of the SJF's rupture front onto the SAF.

B. Modeling approach:

We derived the fault geometries of the SAF and SJF the SCEC Community Fault Model (CFM) version 5.2. We considered 2 configurations for the SJF (Figure 1). In configuration A, the SJF adopts the Middle San Jacinto (MSJ) strand but in configuration B, it takes the Glen Helen (GH) strand which is closer to the SAF. For each of the two geometries, we build a three-dimensional finite element mesh using Trelis software (www.csimsoft.com) where we approximate the faults with non-planar segments and we sample the model space with tetrahedral finite elements. For all geometries, we chose a mesh size of 200 m on the fault planes and allow the mesh to grow geometrically away from the faults. The meshes were then incorporated into the finite

element code FaultMod [Barall, 2009], which has been tested in the SCEC-USGS dynamic rupture code comparison exercise [Harris et al., 2018], to compute the dynamic rupture propagation. We considered a homogeneous elastic medium, a static friction of 0.6 and a dynamic friction of 0.15. We allowed a total dynamic simulation time of 40 s with a time step interval of 0.005 s. We used the regional stress distribution described in Lozos, [2016] with stress orientations of N16W on the northern section of the SAF, N7W on the southern section and N12E on the SJF. Using these maximum horizontal stress orientations, we derived the initial shear and normal stresses on the faults and we also applied a taper in the upper 3 km so that the shear and normal stresses decrease linearly to zero at the free surface. We can notice that the change in geometry of the SJF for geometry A and B does affect the initial shear stress (Figure 2). In geometry A, the shear stress reduces and the normal stress increases on the MSJ section of the San Jacinto strand while this is not the case for the GH portion of the San Jacinto strand for geometry B. This fluctuation of the initial stresses suggest that it will be more likely for the rupture to dies out on the MSJ as opposed to the GH strand. For each of the scenarios, we then evaluated the synthetic seismograms at 5 hypothetical sites on the SAF where surface ground displacement is extracted for dynamic triggering analysis. Those seismograms were used to model the time dependent stress tensors (caused by the seismic waves) and its influence on the receiving segment along the SAF. For a rupture on the SJF, since the seismic waves can propagate faster than the rupture front, they can damage some segments of the SAF. Consequently, when the rupture front moves towards the already damaged SAF, segments of the SAF already damaged by the seismic waves could easily be pushed to failure as opposed to segments which were not damaged. By modeling the dynamic stresses at each of those 5 sites caused by the passing of the seismic waves, we analyzed regions of the SAF that experienced increased in dynamic stresses ahead of the rupture front.

C. Results:

For all the scenarios, we initiated the rupture on the southeastern end of the SJF and we only allowed rupture to reach a depth of 15 km to be consistent with local seismicity (Lin et al., 2007). For scenario 1, we considered a slip weakening distance (SWD) of 0.6 m. For both geometries, the rupture was able to break the SJF entirely but could not propagate from the SJF to the SAF (Figure 3). However, for scenario 2. when we decreased the SWD by 50% (0.3 m), the rupture was only able to jump from the SJF to the SAF for geometry B. The rupture triggers the northern section of the SAF first and then back propagate to the southern section and more slip can observed on the northern section of the SAF. This indicates that a rupture initiated on the SJF is more likely to propagate onto the SAF when the rupture follows the geometry B (SJF adopts the Glen Helen strand) instead of geometry A (SJF adopts the MSJ strand). Under the configuration of geometry B and for the scenario 2, we extracted the synthetic seismograms for the 5 sites (Figure 4) and evaluated the dynamic stress triggering. Figure 5 is showing the time dependent dynamic stresses with depth evaluated at only station 3 which is near the intersection between SAF and SJF. Even though the SAF didn't rupture during this event, the results show a positive dynamic stress of about 4 MPa from the free surface to a depth of 10 km at about 12 seconds, which is then followed by a negative stress of about -3MPa at 16 seconds. Thus, by increasing the radiated energy (swd of 0.3m), the stress changes related to the rupture front at the SJF could be enough to facilitate the propagation of the SJF rupture onto the SAF due to the already damaged segments of the SAF from the dynamic stresses.

D. Summary:

Our results suggest that the passing seismic waves, generated by a rupture in the SJF, has the potential to cause an increase in dynamic stresses on the northern branch of the SAF and damage that section of the fault ahead of the rupture. This could facilitate and trigger slip on the northern branch of the SAF, as described for the scenario 2.

E. Research presentations

Our research was presented in the following meetings/seminars:

SCEC Annual Meeting 2020, Palm Spring, CA:
Gonzalez-Huizar, H., & Douilly, R (2020). Investigating the Role of Seismic Waves on Multi-fault Rupturing. SCEC Contribution 10647, (poster presentation)

Seminar, Department of Geophysics, University of Kyoto, Japan:
Gonzalez-Huizar, H. (2022), *Insight into dynamic triggering of seismicity* (oral presentation)

Mexican Geophysical Union Annual Meeting 2023, Puerto Vallarta, Mexico:
Gonzalez-Huizar, H., & Douilly, R (2023). The Role of Seismic Waves on Multi-fault Rupturing (poster presentation)

F. References

Barall, M., 2009, A grid-doubling finite-element technique for calculating dynamic three-dimensional spontaneous rupture on an earthquake fault: Geophysical Journal International, v. 178, p. 845–859, https://doi.org/10.1111/j.1365-246X.2009.04190.x.

Dolan, J. F. et al. Prospects for larger or more frequent earthquakes in the Los Angeles Metropolitan region. Science 267, 199–205 (1995).

Hill, D. P. (2012a). Dynamic stresses, Coulomb failure, and remote triggering—Corrected, Bull. Seismol. Soc. Am. 102, no. 6, 2313–2336.

Hill, D. P. (2012b). Surface-wave potential for triggering tectonic (nonvolcanic) tremor—Corrected, Bull. Seismol. Soc. Am. 102, no. 6, 2337–2355.

Lin, G., Shearer, P.M., and Hauksson, E., 2007, Applying a three-dimensional velocity model, wave- form cross correlation, and cluster analysis to locate southern California seismicity from 1981 to 2005: Journal of Geophysical Research, v. 112, B12309, https://doi.org/10.1029/2007JB004986.

Lozos, J.C (2016), A case for historic joint rupture of the San Andreas and San Jacinto faults. Sci. Adv. 2, e1500621.

Nissen, E., et al (2016), Limitations of rupture forecasting exposed by instantaneous triggering earthquakes boublet, Nature geo, vol. 9, doi: 10.1038/NGEO2653.

Rubin, C. M. Systematic underestimation of earthquake magnitudes from large intracontinental reverse faults: historical ruptures break across segment boundaries. Geology 24, 989–992 (1996).

Zhang, H, J. Chen, Z. Ge (2012), Multy-fault ruptures ans successive triggering during the 2012 Mw 86 Sumatra offshore earthquake, Geophys. Res.L., vol. 39, L 22305. Doi:10.1029/2012GL053805.

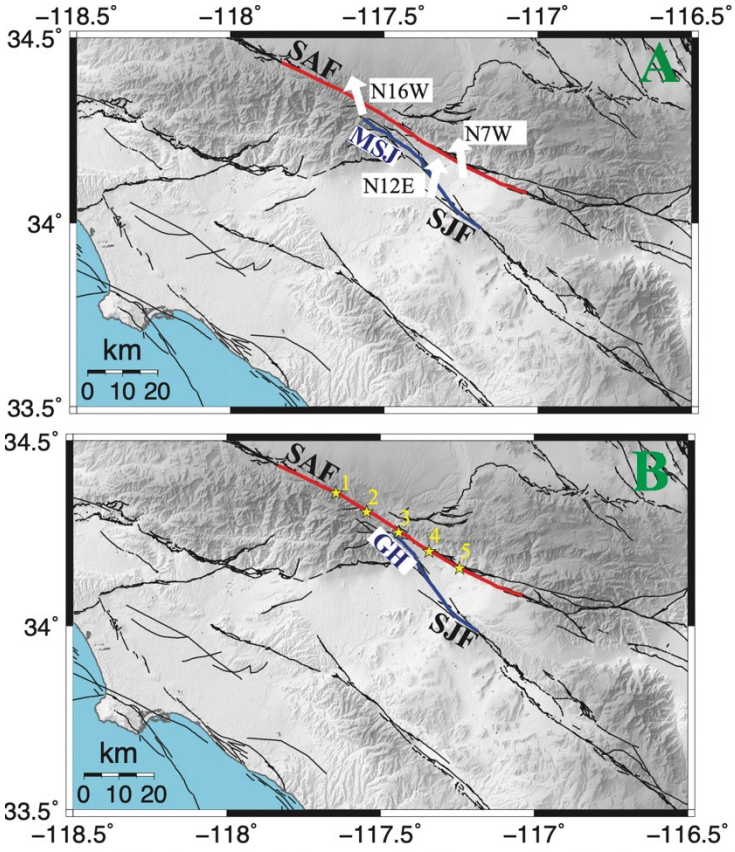

Figure 1: Map view of our study area. The red line is the segment of the SAF that we consider in our simulation and the blue segment represents the SJF. We consider 2 configurations for the SJF. In geometry A, the SJF adopts the MSJ strand and in geometry B the GH strand which is closer to SAF. The fault geometries are derived from the SCEC CFM. The white arrows show the horizontal stress orientation used to derive the initial shear and normal stresses on each fault. The yellow stars represent the sites where surface ground displacement is extracted for the dynamic triggering analysis.

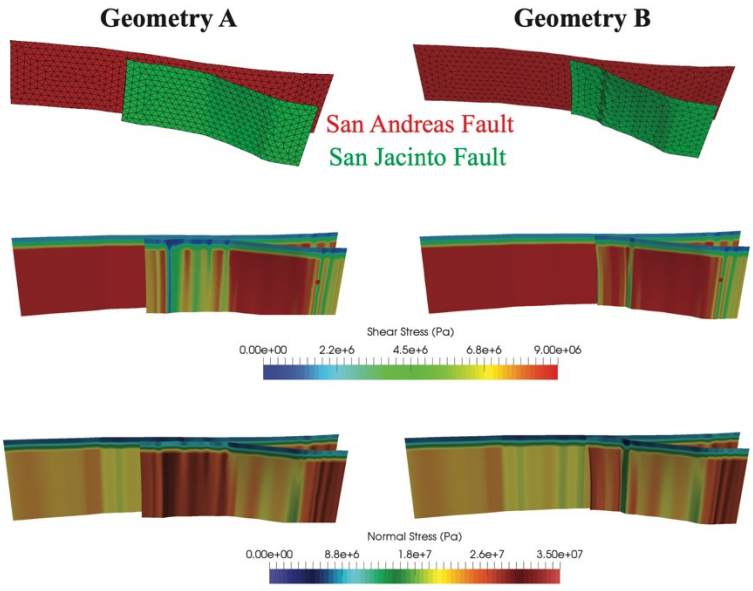

Figure 2: The first line shows a snapshot of the finite element meshes generated from TRELIS for both geometries. The mesh is displayed at a coarser mesh size for visualization purposes. The middle and bottom lines show the initial and normal stresses for geometries A (left) and B (right)

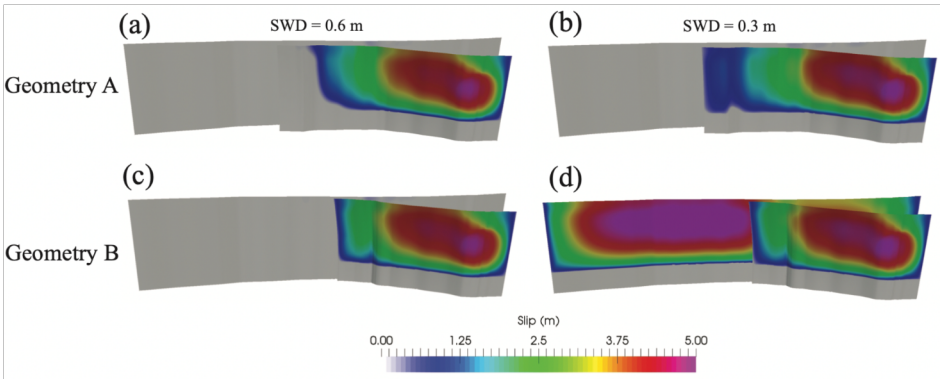

Figure 3: Final slip distribution for geometries A and B for the dynamic models with a slip weakening distance of 0.6 m (1st column) and 0.3 m (2nd column).

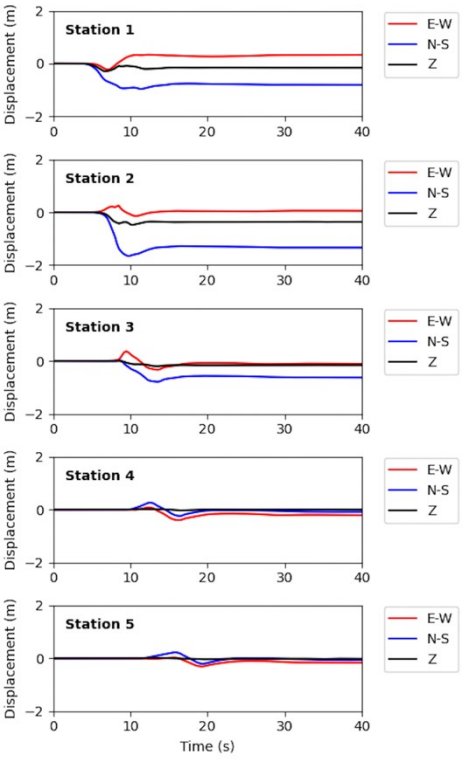

Figure 4: Synthetic seismogram at the five sites along the SAF in Figure 1 (yellow stars) for the rupture simulation with a slip weakening distance of 0.6m on geometry B.

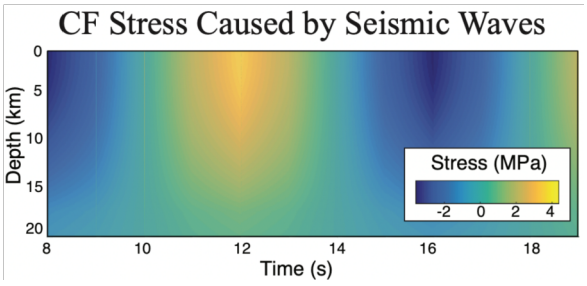

Figure 5: Dynamic stresses caused underneath station 3 by the passing seismic waves as function of depth and time since the rupture initiates at the SJF.